GPPS | JOURNAL

JOURNAL OF THE GLOBAL POWER AND PROPULSION SOCIETY
journal.gpps.global

The effect of working fluid and compressibility on the optimal solidity of axial turbine cascades

Original article

Article history:
Submission date: 6 July 2023
Final revision date: 24 March 2024
Acceptance date: 19 August 2024
Publication date: 4 November 2024

***Correspondence:**
MP: m.pini@tudelft.nl

Peer review:
Single blind

Copyright:
© 2024 Tosto et al. This is an open access article distributed under the Creative Commons Attribution License (CC-BY 4.0), which permits unrestricted use, distribution, and reproduction in any medium, provided the original work is properly cited and its authors credited.

Keywords:
working fluid; solidity; organic Rankine cycle turbines; flow compressibility

Citation:
Tosto F., Colonna P., and Pini M. (2024). The effect of working fluid and compressibility on the optimal solidity of axial turbine cascades. Journal of the Global Power and Propulsion Society. 8: 436–455.
https://doi.org/10.33737/jgpps/192451

Francesco Tosto[1], Piero Colonna[1], Matteo Pini[1,*]

[1]*Propulsion and Power, Faculty of Aerospace Engineering, Delft University of Technology, Kluyverweg 1, HS Delft 2629, The Netherlands*

Abstract

The blade solidity, namely the blade chord-to-pitch ratio, largely affects the fluid-dynamic performance of turbomachinery and its cost. For turbomachines operating with air or steam, the optimal value of the solidity which maximizes the efficiency is estimated with empirical correlations such as the ones proposed by Zweifel (1945) and Traupel (1966). However, if the turbomachine operates with unconventional fluids, the accuracy of these correlations is questionable. Examples of such fluids are the organic compounds (e.g., hydrocarbons, siloxanes) used in organic Rankine cycle (ORC) power systems. This study concerns an investigation on how the working fluid, its thermodynamic state, and flow compressibility influence the optimum pitch-to-chord ratio of turbine stages. A first principle reduced-order model (ROM) for the computation of profile losses was developed for this purpose. The ROM results are compared with those obtained from numerical simulations of the flow over two axial turbine cascade geometries. The influence of both the working fluid, the flow compressibility, and the solidity value on both the boundary layer state at the blade trailing edge and the base pressure are evaluated. Models to compute mixing and passage losses in the compressible regime as a function of the axial solidity are proposed and discussed. Results show that the value of the optimal solidity of turbine cascades significantly increases with the flow compressibility, and mildly increases if the fluid is in the dense vapor state. Moreover, the optimal solidity value is strongly affected by the mixing process occurring downstream of the blade trailing edge. Therefore, currently available models for its estimation, which are solely based on the minimization of the profile losses, are inaccurate.

Introduction

The value of the blade solidity, i.e., the ratio c/s between the chord and the pitch, strongly affects the cost and the performance of axial turbines. To reduce the weight and the cost of the machine, high blade spacing, and low solidity values are desired. However, efficient flow turning requires a sufficient number of blades. For low solidity values, the blade loading is high, causing poor fluid guidance and, therefore, flow separation over the rear suction side. Conversely, for high solidity values, the large cascade wetted area leads to considerable viscous dissipation. In summary, there is an optimum value of the axial solidity, defined as $\sigma_X = c_x/s$, being c_x the axial chord, that minimizes the passage losses. In axial turbines operating with air or steam, this value can be estimated using the empirical correlations proposed by Zweifel (1945) and Traupel (1966). The use of the Zweifel criterion is well documented also in recent literature (Giuffré and Pini, 2021). Although the Zweifel

OPEN ACCESS

correlation is still largely used to estimate the solidity of air, gas, or steam turbines, its accuracy has not been thoroughly assessed in the case of turbines operating with more molecularly complex working fluids. Examples of such fluids are organic compounds, e.g., fluorocarbons, hydrocarbons, or siloxanes, used as working fluids in organic Rankine cycle (ORC) power systems (Colonna et al., 2015; Knowledge Center on Organic Rankine Cycle (KCORC), 2022). These fluids are characterized by large molecular complexity and relatively high critical temperature. Turbines of ORC systems operate with comparatively higher stage expansion ratios than those of more conventional turbines. Moreover, part of the expansion typically occurs in thermodynamic states close to that of the critical point, therefore the flow is affected by non-ideal effects. The magnitude of non-ideal effects in dense vapor flows can be assessed by evaluating the variation of the generalized isentropic pressure-volume exponent (Kouremenos and Antonopoulos, 1987), defined as

$$\gamma_{pv} = -\frac{v}{p}\left(\frac{\partial p}{\partial v}\right)_s = -\frac{v}{p}\frac{c_p}{c_v}\left(\frac{\partial p}{\partial v}\right)_T, \tag{1}$$

where γ is the ratio of the specific heats. If the fluid is in the dense vapor state, the γ_{pv} value changes over the expansion process and the internal flow field substantially depart from that characterizing turbo-machines operating with steam or air. For example, if the fluid is in the dense vapor state, the intensity of shock waves and expansion fans is quantitatively different from that characterizing ideal gas expansions (Romei et al., 2020). Moreover, previous research works (Giuffré and Pini, 2021; Tosto et al., 2021) showed that compressibility effects in turbines operating with the fluid at least partially in the dense vapor state can be enhanced or mitigated depending on whether the γ_{pv} value exceeds that of γ evaluated for ideal gas states (Baumgärtner et al., 2020; Romei et al., 2020).

Moreover, the non-ideality of the flow largely affects the loss breakdown, and, consequently, the blade design. All loss sources, i.e., those associated with viscous effects in boundary layers, with shocks, and with mixing at the blade trailing edge, depend on the thermodynamic state of the fluid and the level of flow compressibility (Giuffré and Pini, 2021). Design parameters, such as the optimal solidity, thus arguably differ from those that would be obtained by applying existing guidelines (Wilson, 1987; Giuffré and Pini, 2021). To the authors' knowledge, no design guideline for the selection of the optimal solidity of turbomachinery operating with non-ideal compressible flows is documented in the literature. The only study on the accuracy of the Zweifel correlation in the case of gas turbines is that of Doughty et al. (1992), who performed an experimental campaign on transonic stator cascades. They found that the Zweifel loading coefficient estimated from their experimental data was significantly higher than the value commonly used to design high-pressure turbine nozzles.

Furthermore, both the Traupel and the Zweifel correlations take into account only the passage loss, while the effects of either wake mixing or shock losses are not considered. As a consequence, the value of the optimal solidity prescribed by these correlations for axial turbines might lead to a sub-optimal design even in the case of steam, air, or gas turbines.

The focus of this study is an investigation of the influence of compressibility, fluid molecular complexity, and thermodynamic non-ideality on the optimal solidity of axial turbine cascades. The research documented in this paper is a first step towards establishing guidelines for the selection of the optimal solidity for the preliminary design of turbomachines operating with non-ideal compressible flows. Based on the approach of Denton (Denton, 1993) and on Coull and Hodson method (Coull and Hodson, 2013), a first-principle reduced-order model (ROM) not requiring the use of empirical coefficients was developed to estimate passage losses as a function of axial solidity. The resulting charts provide the value of optimal solidity as a function of cascade flow angles. Numerical simulations of the flow through two exemplary turbine blades were performed to assess the influence of both flow compressibility and axial solidity on losses and to verify the accuracy of the ROM. Optimal solidity values calculated by taking into account either passage losses alone or the overall loss within the domain are compared with the ones resulting from both the ROM and Zweifel correlation. The influence of the working fluid and its thermodynamic state, flow compressibility, and solidity value on both the boundary layer state at the blade trailing edge and the base pressure is evaluated. Models to evaluate the mixing and the passage losses in the compressible flow regime as a function of the axial solidity are developed and discussed.

The paper is structured as follows. Section 2 describes the approach used to study the effect of solidity on the performance of a turbine cascade. The setup of the computational fluid dynamics (CFD) simulations performed on two representative turbine cascade geometries is also presented. In Section 3, two physics-based reduced-order models (ROMs) for the estimation of the optimal solidity in turbine cascades operating with non-ideal flows, based on the incompressible and compressible flow assumption, respectively, are introduced and described. Section 4 offers a comparison between the results obtained from the CFD and those obtained from the ROMs.

An overview of the limitations of each model is provided, concluding that the models are unsuitable for design purposes. Based on the CFD results, the influence of the flow field in the proximity of the blade trailing edge and in the mixing region on the optimal solidity is also discussed. Finally, Section 5 lists the main conclusions drawn from this study and outlines possible next steps.

Effect of solidity on cascade performance

The effect of solidity on the fluid dynamic performance of turbine cascades can be investigated, either numerically or experimentally, with three different methods: (1) by changing the blade solidity and optimizing its shape for minimum loss at each operating condition; (2) by changing the solidity for a fixed blade shape, but keeping constant the throat-to-spacing ratio for given operating conditions, thus varying the stagger angle of the cascade; (3) by solely changing the solidity, while keeping the blade shape fixed, and varying the operating conditions. This study is numerical and based on the second method. This method enables one to arguably achieve aerodynamic similarity regardless of the solidity value and without re-designing the blade. Following the same approach proposed by Doughty et al. (1992), the blade is rotated about the trailing edge to keep the gauge angle constant, regardless of the solidity value, see Figure 1. The gauge angle χ is defined as

$$\chi = \arccos\left(\frac{o}{s}\right), \tag{2}$$

where o denotes the throat length.

In turbine cascades, passage losses are not the only contribution to the overall loss. The solidity can arguably have an effect also on the mixing process occurring downstream of the blade trailing edge which, in turn, contributes to the overall irreversible entropy generation across the cascade. As pointed out by Denton (1993), mixing losses depend on the base pressure coefficient, as well as on the displacement and momentum thickness at the trailing edge of the boundary layers developing on the pressure and suction sides. For a compressible flow, mixing losses are also a function of the kinetic energy thickness of the boundary layer. With reference to the control volume shown in Figure 2, where the subscript e denotes the station at which the flow is completely mixed-out, the mass, axial momentum, tangential momentum, and energy conservation equations for the mixing

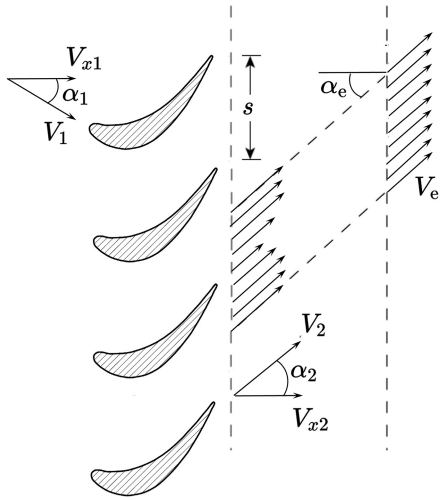

Figure 1. Control volume for the estimation of the mixing losses downstream of the blade trailing edge.

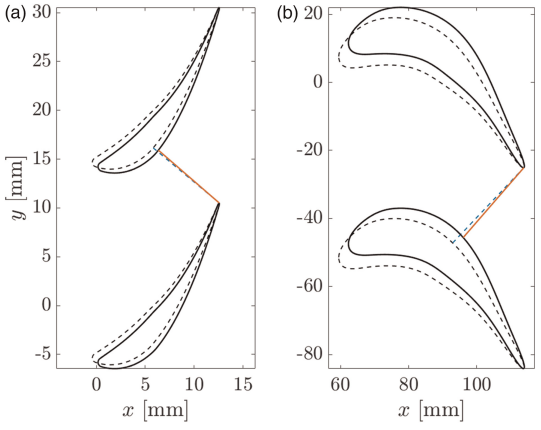

Figure 2. Geometric rotation of the blades about the trailing edge used to obtain the value of optimal solidity for (see nomenclature of Table 1) the (a) *iMM-Kis3* and (b) Aachen turbine blades. Solid lines denote the original geometries, dashed lines are the rotated geometries. The throat length (orange: original geometry, dashed blue: rotated geometry) is varied accordingly to the solidity value to keep the gauge angle constant.

process occurring downstream of a turbine cascade read

$$\rho_2 V_2 \cos\alpha_2 \left(1 - \frac{\delta^* + t}{s}\right) = \rho_e V_e \cos\alpha_e = \dot{m}, \tag{3}$$

$$p_e - p_2 = C_{pb}\frac{t}{s}(p_{t2} - p_2) + \rho_2 V_2^2 \left(1 - \frac{\theta}{s} - \frac{\delta^* + t}{s}\right)\cos^2\alpha_2 - \rho_e V_e^2 \cos^2\alpha_e, \tag{4}$$

$$\rho_2 V_2^2 \left(1 - \frac{\theta}{s} - \frac{\delta^* + t}{s}\right)\cos\alpha_2 \sin\alpha_2 = \rho_e V_e^2 \cos\alpha_e \sin\alpha_e, \tag{5}$$

and

$$\dot{m}\left(h_2 + \frac{V_2^2}{2}\right) - \rho_2 \frac{V_2^3}{2}\theta^* = \dot{m}\left(h_e + \frac{V_e^2}{2}\right). \tag{6}$$

In the equations, δ^*, θ, and θ^* denote the displacement, momentum, and kinetic energy thickness, respectively, and p_b the base pressure. The base pressure is expressed in terms of the so-called *base pressure coefficient*, defined as

$$C_{pb} = \frac{p_b - p_2}{p_{t2} - p_2}, \tag{7}$$

where p_{t2} is the stagnation pressure at the exit of the vane. For an incompressible flow, an analytical equation for the loss within the domain can be obtained by simplifying Equations 3–5. The total pressure-based loss coefficient is (Denton, 1993)

$$\zeta_{inc} = \frac{p_{t1} - p_{t2}}{(1/2)\rho V_1^2} = -C_{pb}\frac{t}{s} + 2\frac{\theta}{s} + \left(\frac{\delta^* + t}{s}\right)^2 \tag{8}$$

From these equations, it emerges that the base pressure coefficient and the boundary layer integral quantities strongly influence the mixing process and associated losses, ultimately affecting the optimal solidity value.

Setup of the CFD simulations

To assess the influence of the axial solidity σ_x on the fluid-dynamic losses, we performed a set of steady-state Reynolds Averaged Navier-Stokes (RANS) simulations of the flow around two blades characterized by different geometrical features. In agreement with the established practice of evaluating the profile losses, to whom the solidity strongly depends, at the blade midspan, two-dimensional computations are deemed sufficient for the scope of this research. Figure 3 shows the computational domain of the two blade geometries. The first blade geometry, hereafter referred to as *iMM-Kis3*, is the mid-span section of the turbine stator also considered in the study documented in Giuffré and Pini (2021). This turbine stage has been designed to operate with hexamethyldisiloxane, commonly referred to as siloxane MM, at inlet total temperature and pressure ensuring a compressibility factor of $Z \sim 1$, i.e., in dilute gas conditions. In this analysis, only the fluid-dynamic performance parameters calculated at the mid-span section have been considered. The baseline design of the stator consists of 42 blades featuring an axial solidity value of $\sigma_{x,\mathrm{ref}} = 0.73$. This value has been calculated using the Zweifel criterion in the preliminary design phase, see Giuffré and Pini (2021). The second blade geometry is the mid-span section of the rotor of the so-called *Aachen* turbine (Stephan et al., 2000), which is representative of highly-loaded cascades. This is the case of, e.g., axial turbines of organic Rankine cycle power plants. The rotor of the *Aachen* turbine was designed to operate with air at a rotational speed of 3,500 rpm and a mass flow rate of $\dot{m} = 6.8$ kg/s. The baseline design consists of 41 blades featuring an axial solidity value of $\sigma_{x,\mathrm{ref}} = 1.3$. Table 1 lists the main geometrical specifications of both blades. Compared to the *iMM-Kis3* blade, the *Aachen* blade is front-loaded, i.e., characterized by a larger thickness in the proximity of the leading edge, whereas the *iMM-Kis3* is aft-loaded. Moreover, in the *Aachen* blade, the extension of the straight part of the rear suction side is longer, the trailing edge is thicker, and the leading edge is more rounded than in the *iMM-Kis3* blade.

To achieve constant χ for all axial solidity values, both blades are rotated around the trailing edge. Figure 1 illustrates the geometrical rotation of both blades. The inlet and the outlet of both domains have been placed $\sim 1.5c_x$ upstream of the leading edge and $\sim 3.5c_x$ downstream of the trailing edge, respectively to avoid upstream

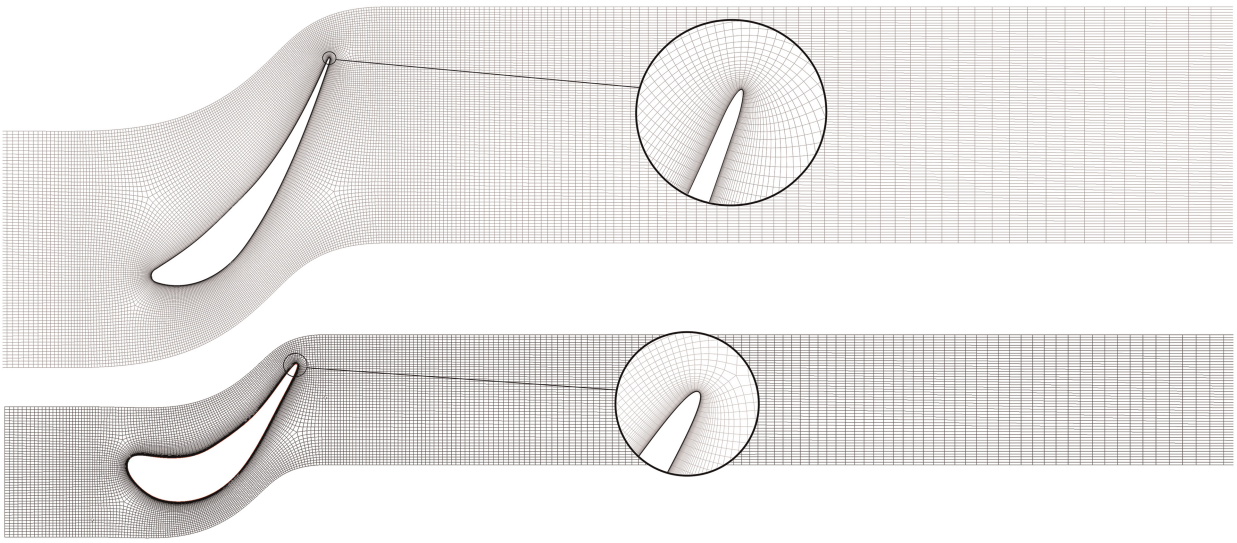

Figure 3. Computational grid for (a) the *iMM-Kis3*, an ORC vane expanding MM in the ideal gas state, and (b) the Aachen turbine blades. The axial solidity is the value at design conditions, i.e., $\sigma_{x,\mathrm{ref}}$. Only one of every four grid lines is shown.

Table 1. Key features of the *iMM-Kis3* and of the Aachen turbine blades.

	c (m)	c_x (m)	γ (°)	s (m)	α_1	α_m (°)	t (mm)	$M_{\mathrm{out},d}$
iMM-Kis3	0.0205	0.0126	50.72	0.0172	0	68.84	0.054	1.3
Aachen	0.0634	0.0543	31.04	0.0418	28.8	71.41	1.405	0.3

γ, α_m, t, and $M_{\mathrm{out},d}$ denote the blade stagger angle, the blade metal angle at the trailing edge, the trailing edge thickness, and the design outlet Mach number, respectively. For the Aachen blade, $M_{\mathrm{out},d}$ refers to the relative Mach number at the rotor outlet.

effects and to let the flow mix for several chord lengths downstream of the blade. Three sets of simulations per blade are considered, each characterized by a different working fluid: for the simulations denoted with iN_2, the working fluid is nitrogen, a compound formed by simple molecules, while for those denoted with *iMM* and *niMM*, the working fluid is siloxane MM, an organic compound used as the working fluid in several ORC turbogenerators. The inlet total temperature and pressure of the iN_2 and *iMM* test cases are prescribed to ensure that the compressibility factor at the inlet is equal to one (ideal gas), while the inlet thermodynamic state of the *niMM* test case is that of a dense vapor, i.e., of a fluid operating in the proximity of the vapor-liquid saturation line. Table 2 lists the boundary conditions for each set of simulations.

To investigate the influence of compressibility on the optimal solidity value, three different values of the total-to-static expansion ratio β_{ts} are considered for each case. The first β_{ts} value leads to subsonic downstream Mach numbers ($M_{\mathrm{out}} \sim 0.5$, M_{out} being the Mach number at the outlet of the domain), the second one leads to transonic flow ($M_{\mathrm{out}} \sim 1$), while the third one is set to achieve supersonic flow ($M_{\mathrm{out}} \sim 1.2$). For each value of β_{ts}, 16 different values of the axial solidity, ranging from $\sigma_x = 0.5$ to $\sigma_x = 1.6$ and from $\sigma_x = 0.6$ to $\sigma_x = 1.6$ for the *iMM-Kis3* and the *Aachen* blades, respectively, are considered.

The domain is meshed with quadrilateral elements using a commercial program for turbomachinery blade meshing (ANSYS, 2019). A grid is generated for each value of the axial solidity σ_x, resulting in 8 different meshes for each of the two blades. Cell clustering is introduced near the blade walls to guarantee $y^+ < 1$. Figure 4 shows the results of the mesh sensitivity analysis for the baseline *iMM-Kis*3 blade ($\sigma_{x,\mathrm{ref}} = 0.73$). The graph shows that the deviation in the value of the overall entropy loss coefficient ζ_s, defined as

$$\zeta_s = \frac{T_2(s_2 - s_1)}{h_{\mathrm{t},2} - h_2}. \tag{9}$$

Table 2. Setup of the numerical test cases. γ_∞ denotes the ratio of specific heats for $v \to \infty$.

iMM-Kis3	M_{mol} (kg/kmol)	γ_∞	p_{t1} (bar)	T_{t1} (K)
iN2	28	1.4	15	473.15
iMM	162.38	1.025	9.66	534.26
niMM	162.38	1.025	25.1	542.04
Aachen	M_{mol} (kg/kmol)	γ_∞	p_{t1} (bar)	T_{t1} (K)
iN2	28	1.4	15	473.15
iMM	162.38	1.025	9.66	534.26
niMM	162.38	1.025	25.1	542.04
iMM-Kis3	$\mathrm{Re}_{2,is} \cdot 10^6$	$\beta_{ts,1}$	$\beta_{ts,2}$	$\beta_{ts,3}$
iN2	1.75–2.50	1.2	2	2.6
iMM	4.47–6.29	1.2	1.7	2.2
niMM	12.1–17.63	1.075	1.5	2.2
Aachen	$\mathrm{Re}_{2,is} \cdot 10^6$	$\beta_{ts,1}$	$\beta_{ts,2}$	$\beta_{ts,3}$
iN2	5.38–7.63	1.2	2	2.6
iMM	15.89–18.85	1.15	1.7	2.2
niMM	37.26–50.91	1.075	1.5	2.2

The Reynolds number is computed using the blade chord c and the isentropic outlet conditions as reference. The last three columns list the values of three total-to-static expansion ratios investigated in each case.

between the 320 k and the 640 k cells meshes is 0.1%. For this study, the 320 k cells mesh ensures the best compromise between accuracy of the results and computational cost. All the mesh parameters, e.g., the growth rate of the cells in the proximity of the walls or the average cell size, are fixed and equal to those used for the baseline mesh also for the remaining 7 computational domains of the *iMM-Kis3* blade, which differ only in the value of the solidity and the related geometry rotation. The same mesh parameters have also been fixed for the *Aachen* blade mesh: at $\sigma_{x,\mathrm{ref}} = 1.3$, the resulting mesh size consists of 440k cells.

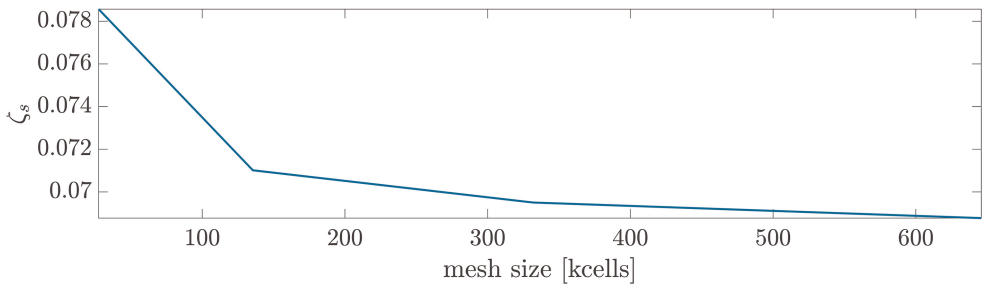

Figure 4. Variation of the overall dissipation coefficient ζ_s (Equation 9) as a function of the number of grid cells for the *iMM-Kis3* test case.

A commercial CFD software (ANSYS, 2019) has been used to simulate the flow through the turbine cascades. The SST $k-\omega$ model (Menter, 1994) has been employed to compute the turbulence stresses. Stagnation pressure, stagnation temperature, and turbulent intensity are prescribed at the inlet, according to the values reported in Table 2. A turbulent intensity value of 5% and a turbulent viscosity ratio μ_T/μ equal to 10 were specified for all simulations. The turbulent Prandtl number was set to $\mathrm{Pr}_t = 0.9$, in accordance with the indications listed in Otero et al. (2018). The advective fluxes were discretized with a second-order accurate scheme. First-order upwind schemes were instead used to discretize turbulent fluxes. Fluid properties are calculated with a look-up table method and tabulated values were computed with a well-known program (Lemmon et al., 2018).

Reduced-order models for the estimation of the optimal solidity

Based on the approach proposed by Denton (1993), two physics-based reduced-order models for the estimation of the optimal solidity in axial turbines have been developed. Both models are based on a simplified blade loading distribution and provide an estimation of the chord-to-pitch ratio value at which the passage loss is minimized. The first model (*iSol*) is applicable to incompressible flows, whereas the second (*cSol*), is its extension to compressible flows. Results obtained from these models are then compared against those obtained from the Zwifel criterion and from the CFD simulations.

Zweifel criterion

The Zweifel criterion is based on the results of experimental campaigns conducted on subsonic turbine linear cascades. The model, in its most general form, reads

$$Z_{Zw} = \frac{\text{actual blade loading}}{\text{ideal blade loading}} = \frac{\rho V_x (V_{y2} - V_{y1})}{(p_{t1} - p_2)\sigma_x}, \tag{10}$$

where ρ is the fluid density, p_{t1} the inlet total pressure, p_2 the outlet static pressure, V_{y1} and V_{y2} the tangential velocities at inlet and outlet, respectively, and V_x the average axial velocity. Z_{Zw} is a coefficient whose value ranges between 0.8 and 1.1 depending on the type of turbine and its application. For example, the Zweifel coefficient of low-pressure turbine stages of modern aircraft engines is approximately 1.1. For an incompressible flow, the correlation reads

$$\sigma_x = \frac{2\cos^2\alpha_2}{Z_{Zw}}(\tan\alpha_2 - \tan\alpha_1), \tag{11}$$

where α_1 and α_2 are the inlet and outlet flow angles.

Physics-based model for incompressible flows (*iSol*)

The incompressible physics-based model has been developed by assuming an exemplary turbine blade geometry (Figure 5a) whose loading is described by the simplified velocity distribution shown in Figure 5b. The flow angles at the inlet and the outlet of the vane are α_1 and α_2, respectively, while δ is the deviation from the outlet metal angle α_m. The blade features a parabolic camber line with a slope at both the leading and the trailing edge equal to the tangent of the flow angles. These assumptions result in the geometric relation

$$\frac{y}{c_x} = -\frac{x}{c_x}\left(A\frac{x}{c_x} + B\right), \tag{12}$$

with $A = (\tan\alpha_2 - \tan\alpha_1)/2$ and $B = \tan\alpha_1$. The blade thickness is assumed negligible, as well as the flow deviation downstream of the blade trailing edge due to the incompressible flow assumption. Even if, in an actual turbine, the thickness distribution determines the blade loading, this assumption is deemed satisfactory for the given purposes. The velocity distribution, and, consequently, the blade loading, depend on the flow velocities V_1 and V_2 at the inlet and the outlet of the cascade. For an incompressible flow, V_1 and V_2 can be calculated knowing the axial velocity V_x, which is constant along the vane, and the flow angles α_1 and α_2. For a given set of flow angles and a given V_x, the blade loading solely depends on the values of the parameters k and $\mathrm{d}V$, which are independent of V_1 and V_2.

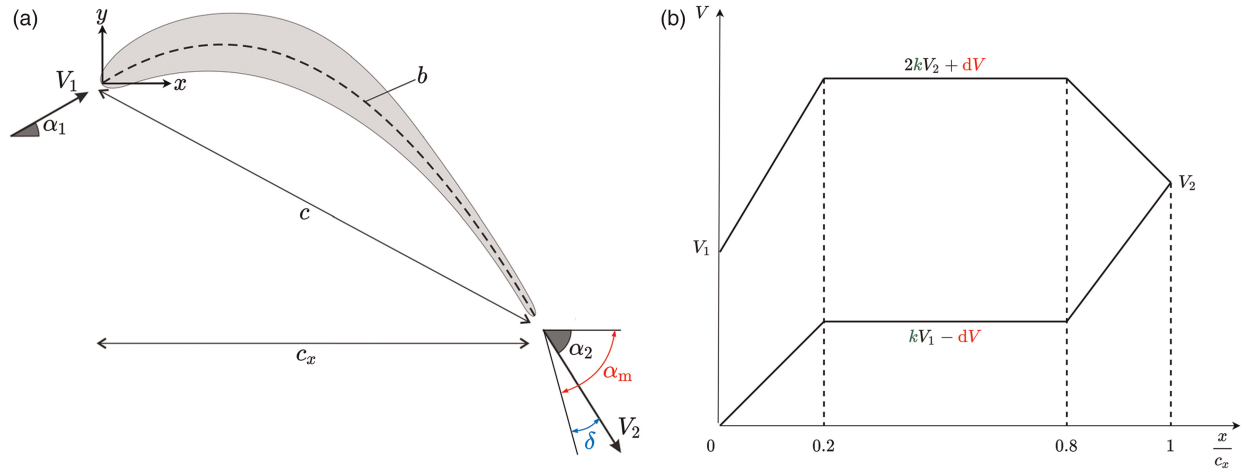

Figure 5. (a) Reference blade geometry for the reduced-order model. Blade thickness is neglected in this study. Adapted from Coull and Hodson (2013). (b) Simplified velocity distribution along the blade axial direction.

The circulation around the blade suction and pressure sides is equal to that around a control volume encompassing the inlet, outlet and the periodic mid-line of the vane, i.e.,

$$\int_0^1 (V_{ss} - V_{ps}) \sqrt{1 + \left(2A\frac{x}{c_x} + B\right)^2}\, \mathrm{d}\left(\frac{x}{c_x}\right) = \frac{(V_2 \sin\alpha_2 - V_1 \sin\alpha_1)}{\sigma_x}, \tag{13}$$

where V_{ss} and V_{ps} are the values of the absolute velocity along the suction and pressure sides, respectively, and are defined by the distribution shown in Figure 5b. The equation for the balance of the tangential momentum reads

$$\int_0^1 (V_{ss}^2 - V_{ps}^2) \mathrm{d}\left(\frac{x}{c_x}\right) = \frac{2V_\mathrm{x}}{\sigma_x}(V_2 \sin\alpha_2 - V_1 \sin\alpha_1) = \frac{2V_\mathrm{x}^2}{\sigma_x}(\tan\alpha_2 - \tan\alpha_1). \tag{14}$$

The pairs of k and $\mathrm{d}V$ values satisfying Equations 13 and 14 can be calculated by eliminating σ_x from the system of equations. For given values of the inlet and outlet flow angles, the optimal solidity value can finally be calculated by minimizing the normalized dissipation due to passage losses, defined as

$$\zeta_P = \frac{T_2 \dot{S}_P}{1/2\dot{m}V_\mathrm{x}^2} = \frac{2C_\mathrm{d}\sigma_x}{V_\mathrm{x}^3} \int_0^1 (V_{ss}^3 - V_{ps}^3) \sqrt{1 + \left(2A\frac{x}{c_x} + B\right)^2}\, \mathrm{d}\left(\frac{x}{c_x}\right), \tag{15}$$

where C_d is the average boundary layer dissipation coefficient over the blade. Following Denton (1993), C_d was assumed constant and equal to 0.002. Equation 15 takes thus into account only the contribution due to dissipation in the boundary layers developing over the blade, the contribution due to mixing and shock waves being neglected. Unlike the Zweifel correlation, the *iSol* model does not require any empirical closure coefficient, but only the values of the inlet and outlet flow angles, arguably ensuring improved accuracy.

Physics-based model for compressible flows (*cSol*)

To provide better estimations in the transonic and supersonic regimes, the incompressible model *iSol* has been modified to treat also compressible flow cases. In contrast to the incompressible case, the axial velocity is not constant but changes with the fluid density according to the mass conservation equation. Moreover, the thermodynamic and kinematic fields are now coupled, and the energy conservation equation is necessary to close the problem. Besides the flow angles α_1 and α_2, the model thus also requires as input the values of the inlet stagnation temperature T_{t1} and pressure p_{t1}, which fix the thermodynamic state of the fluid, and the total-to-static expansion ratio β_{ts}.

The *cSol* model is developed starting from the same simplified blade geometry described in Section 2 and shown in Figure 5. The blade loading is calculated by integrating the simplified pressure distribution over the pressure and suction sides depicted in Figure 6a, which varies according to the values of the two parameters c

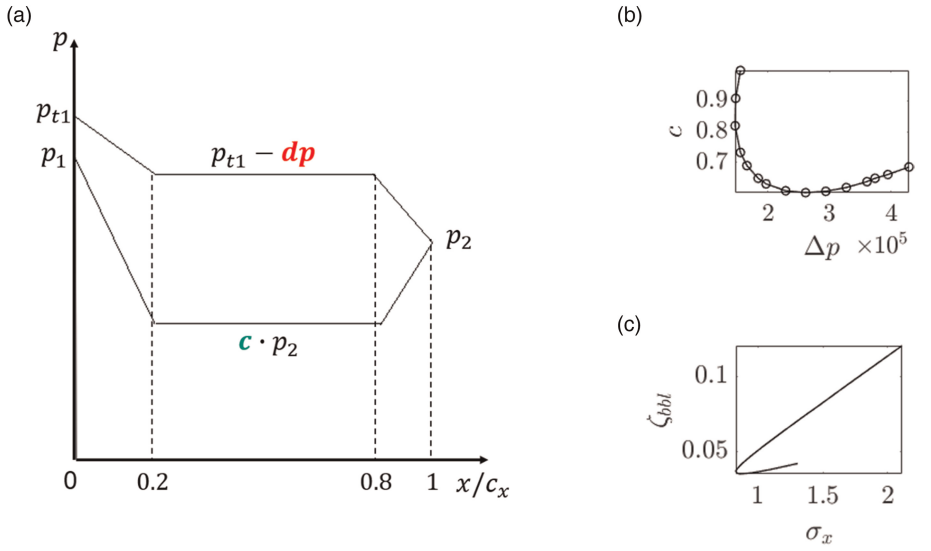

Figure 6. (a) Simplified pressure distribution along the blade axial direction. (b) Locus of c and Δp values satisfying Equations 13, 16 and 17 (c) Dissipation due to losses in the passage vs σ_x computed for the c and Δp values shown in graph (b). For graphs (b) and (c), $\alpha_1 = 0°$, $\alpha_2 = 68.84°$, $\beta_{ts} = 1.4$. The thermodynamic inlet conditions match those of the iMM case.

and dp. The total pressure p_{t1} and the static pressures p_1 and p_2 define the values of the pressure distribution at the leading and trailing edge: the outlet pressure p_2 is retrieved from the expansion ratio $\beta_{ts} = p_{t1}/p_2$. The inlet density ρ_1 value is set to $0.97\rho_{t1}$, while the entropy at the outlet is set to $s_2 = 1.0001s_1$. These values have been chosen by averaging those obtained from the results of the CFD simulations performed on the *iMM-Kis3* blade and described in Section 2. By fixing the inlet density and the outlet entropy, it is possible to estimate the trends of pressure, velocity and enthalpy along the blade. A sensitivity analysis on ρ_1 and s_2 has been conducted, resulting in a negligible influence on the values of the optimal solidity. The compressible form of the tangential momentum balance can be expressed as

$$\int_{(l_{ss}+l_{ps})} pn \cdot \frac{\mathrm{d}l}{c_{ax}} = \frac{\dot{m}}{s} \frac{V_2 \sin\alpha_2 - V_1 \sin\alpha_1}{\sigma_x}, \tag{16}$$

where p is the pressure over the blade. The energy conservation equation for streamlines following the blade pressure and suction side is given by

$$h_{t1} = h_{ps} + \frac{V_{ps}^2}{2} = h_{ss} + \frac{V_{ss}^2}{2}. \tag{17}$$

The combination of Equation 17 with the fluid thermodynamic model allows the velocity distribution over the blade to be retrieved from the pressure distribution. In this study, the thermodynamic properties of the fluid are calculated using a well-known program (Lemmon et al., 2018). The blade circulation equation (Equation 13), which also holds in the compressible flow case, closes the system of equations. For a given set of flow angles and boundary conditions, there are infinite combinations of c and dp values satisfying Equations 13, 16 and 17. The locus of such c and dp combinations is shown in Figure 6b. The dissipation due to passage losses, which reads

$$\zeta_P = \frac{T_2 \dot{S}_P}{(1/2)\,\dot{m} V_2^2}, \tag{18}$$

where

$$\dot{S}_P = \int_{l_{ps}} \frac{C_d \rho_{ps} V_{ps}^3}{T_{ps}} \mathrm{d}l + \int_{l_{ss}} \frac{C_d \rho_{ss} V_{ss}^3}{T_{ss}} \mathrm{d}l, \tag{19}$$

is calculated for each combination of c and $\mathrm{d}p$ satisfying Equations 13, 16 and 17. The optimal solidity value corresponding to the minimum loss (Figure 6c) is then evaluated.

Comparison of model results

Figure 7a–c show the loss breakdown for the *iMM-Kis3* blade obtained from the results of the CFD simulations, see Section 2. Each loss source is plotted as a function of the axial solidity for the iN_2, *iMM* and *niMM* cases, respectively, and for each value of the outlet Mach number corresponding to the β_{ts} reported in Table 2. The loss coefficient $\zeta_s = T_2 \Delta s / u_2^2/2$, where the reference temperature and the flow velocity are computed at the outlet boundary, is used to quantify the dissipation produced by each loss source. For all cases, the red and

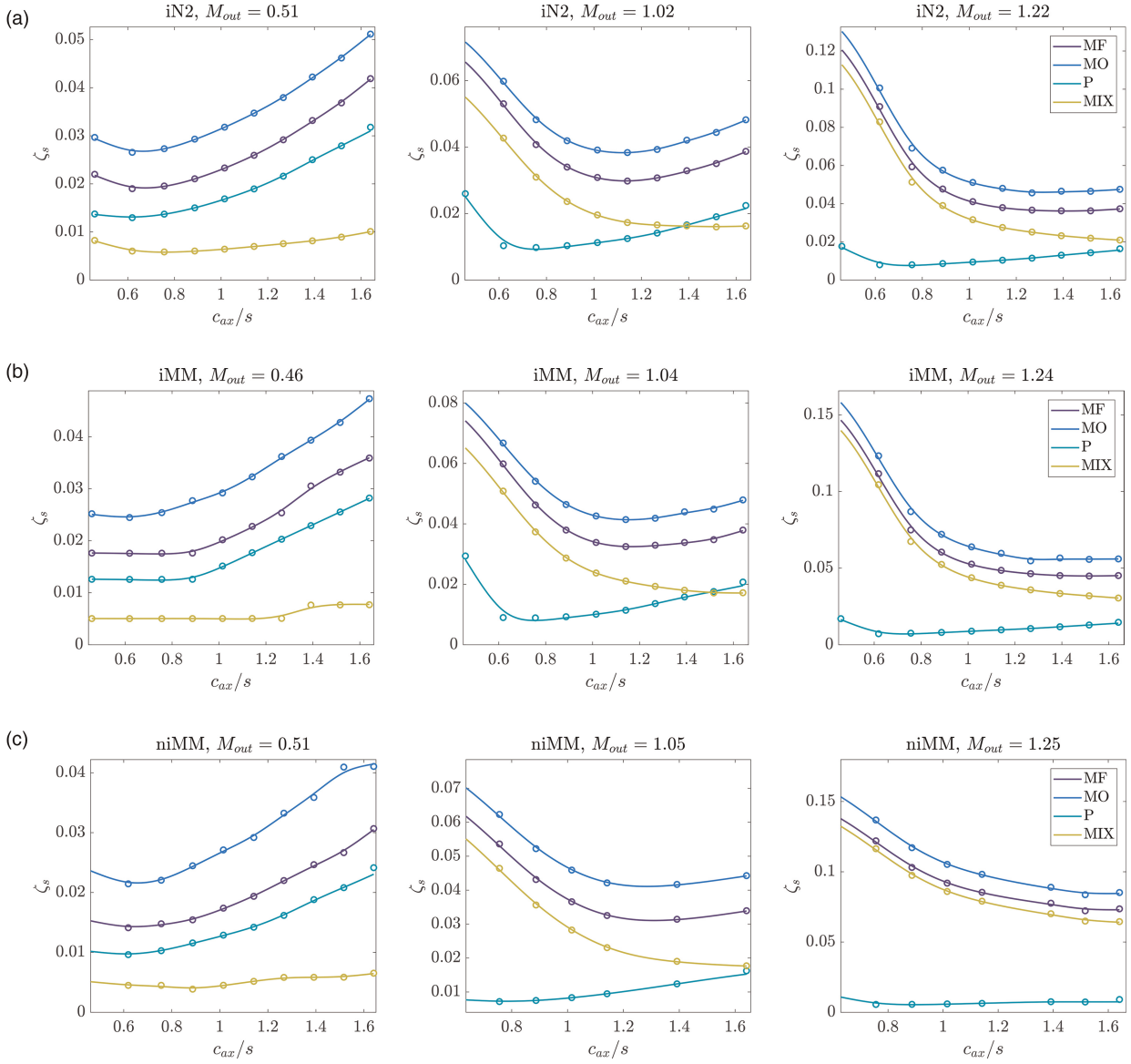

Figure 7. Normalized entropy generation vs blade axial solidity for the *iMM-Kis3* blade. (a) iN_2, (b) iMM, and (c) niMM. Left graphs - subsonic, centre graphs - transonic, right graphs - supersonic outlet Mach number. MF: overall mass-flow averaged loss; MO: overall mixed-out averaged loss; P: passage loss; MIX: mixing loss downstream of the blade trailing edge.

the black curves provide the overall entropy increase between the inlet and the outlet of the computational domain, calculated using both mass-flow (MF) and mixed-out (MO) averaging techniques, respectively. The contribution due to the passage losses (P) is calculated as the difference in mass-flow averaged entropy between the inlet section of the computational domain and a section placed in proximity of the trailing edge at $x = 0.98c_x$. The loss due to mixing (MIX) downstream of the blade trailing edge, instead, is obtained by subtracting the passage loss from the overall mass-flow averaged one.

Results show that the optimal solidity value increases with the flow compressibility, i.e., with the cascade Mach number, regardless of the working fluid and the thermodynamic conditions. At subsonic operating conditions ($M_{\text{out}} \sim 0.5$, left graphs on Figure 7a–c), passage losses prevail over the mixing ones and determine the value of the solidity at which the overall losses are minimized. For all the investigated cases, both the passage and the overall MF and MO averaged losses exhibit a minimum at $\sigma_{x,\text{opt}} \sim 0.65$, and no influence of the fluid and its thermodynamic state is observed. At transonic and supersonic M_{out} values (centre and right graphs in Figure 7a–c, respectively), mixing losses increase and prevail over the passage ones. Therefore, the optimal solidity value now strongly depends on the trend of the mixing losses. In the supersonic regime, in particular, a monotonically decreasing trend of the mixing losses with σ_x is observed for all the investigated cases. Conversely, little deviations are observed in the value of σ_x minimizing the passage losses ($0.65-0.75$ for all the investigated cases). At fixed solidity and operating conditions, larger mixing losses are observed if the expansion occurs in a complex organic compound (*iMM* and *niMM* cases) rather than in a fluid made of simple molecules (iN_2 case), and the overall loss is minimized at larger $\sigma_{x,\text{opt}}$ values. The increase in mixing losses is even larger if the organic fluid is operated in the dense vapor state (*niMM* cases). In the transonic regime (central graphs in Figure 7a–c), the $\sigma_{x,\text{opt}}$ value at which the overall MF and MO losses are minimized is ~ 1.15 for the iN_2 and the *iMM* cases, and 1.25 for the *niMM* case. In the supersonic regime (graphs on the right in Figure 7a–c), instead, the $\sigma_{x,\text{opt}}$ value is found within the range $1.2-1.3$ for the iN_2 case, $1.3-1.5$ for the *iMM* case, and $1.5-1.6$ for the *niMM* case. However, for the supersonic *niMM* case (Figure 7b, on the right), the MF and MO averaged losses are arguably insensitive to variations of axial solidity in the proximity of $\sigma_{x,\text{opt}}$: a lower blade number could thus be used for this case, without sensibly affecting the performance of the cascade.

Figure 8 shows the loss breakdown for the *Aachen* blade. Despite the blade being characterized by a larger flow turning and, consequently, a higher loading, the observed trends match those obtained for the *iMM-Kis3* blade: the $\sigma_{x,\text{opt}}$ value minimizing the overall MF and MO losses increases with M_{out}, and the share of the mixing losses on the overall loss increases with M_{out}, exhibiting a decreasing monotonic trend with σ_x at supersonic regimes (right graphs in Figure 8a–c). Depending on the flow regime, the passage losses are minimized at different values of σ_x: if $M_{\text{out}} < 1$ (left graphs in Figure 8a–c), the minimum is observed at $\sigma_x \sim 0.6$, while in the transonic and supersonic cases, the same minimum occurs at $\sigma_x \sim 1$ (centre and right graphs in Figure 8a–c). Note that an optimal solidity value for the *niMM* case in the highly transonic regime (rightmost graph in Figure 8c) has not been found: mixing losses are arguably minimized at larger σ_x values than those investigated in this study.

The physical reason that allows explaining the trends of the losses as a function of the solidity value can be obtained by inspecting the entropy contours of the *iMM-Kis3* blade displayed in Figure 9a–c. The contour plots refer to the *iMM* case at $\beta_{ts} = 1.7$ or, equivalently, $M_{\text{out}} \sim 1$. At $\sigma_x \sim 0.65$ (Figure 9a), the passage loss is minimized because of the low overall wetted area. However, the poor flow guidance provided by the blades causes flow diffusion on the rear part of the suction side, which entails a considerable boundary layer growth in the vicinity of the trailing edge. As a result, losses are significantly high due to the mixing of a higher portion of low momentum flow with the core flow. At $\sigma_x \sim 1.05$ (Figure 9b), the wetted area increases, leading to an increase of the passage loss. However, mixing losses are lower than in the $\sigma_x \sim 0.65$ case due to the reduction of the flow diffusion in the rear suction side, thanks to the improved flow guidance. At $\sigma_x \sim 1.4$ (Figure 9c), the magnitude of the passage losses equals that of the mixing one, leading to an overall increase of the loss coefficient. The same physical explanation, albeit with a different share of the losses, also applies to supersonic cases. The effect of the solidity on the wake at the blade trailing edge is also visible in the Mach number contours, see Figure 10. The Mach number contour plots also highlight the presence of a shock wave in the proximity of the trailing edge. Similar considerations hold for the *Aachen* blade (not shown).

The previous discussions mostly focused on the results obtained from the CFD. In the following, the results obtained with the reduced-order models described in Section 3 are presented. Figure 11a–f depict the trends of the optimal solidity value as a function of the M_{out} for the *iMM-Kis3* and the *Aachen* blades. Values of $\sigma_{x,\text{opt}}$ calculated considering the overall MF and MO loss, and the passage losses only are reported in the charts. The optimal solidity values calculated with the Zweifel criterion assuming $Z_{Zw} = 0.85$, $Z_{Zw} = 0.95$ and $Z_{Zw} = 1.1$, and that estimated by the *iSol* model are also depicted. For both models, $\alpha_2 = \alpha_m$, α_m being the outlet blade metal angle.

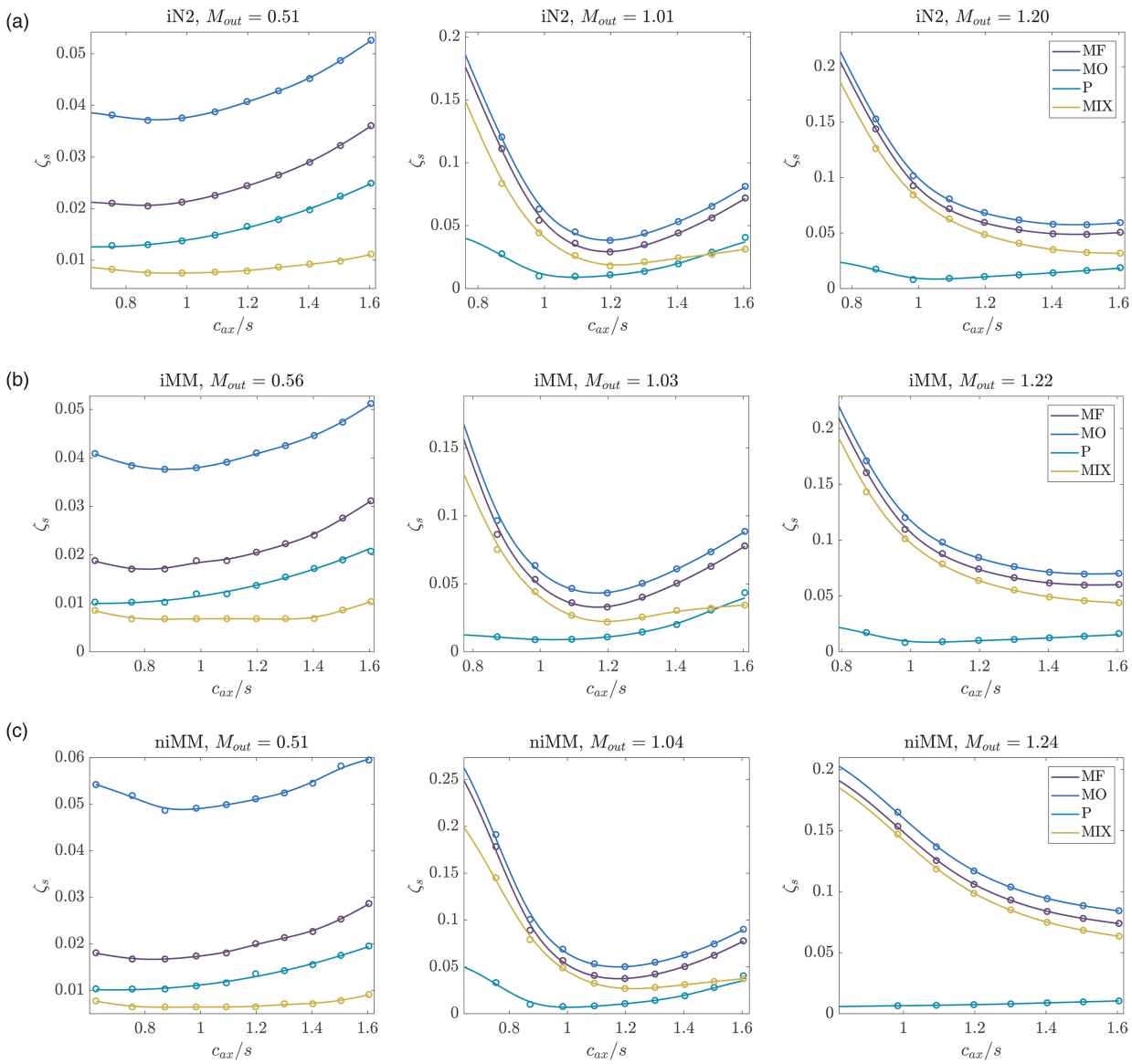

Figure 8. Normalized entropy generation vs blade axial solidity for the Aachen blade. (a) iN_2, (b) iMM, and (c) niMM. Left graphs - subsonic, centre graphs - transonic, right graphs - supersonic outlet Mach number. MF: overall mass-flow averaged loss; MO: overall mixed-out averaged loss; P: passage loss; MIX: mixing loss downstream of the blade trailing edge.

For transonic and supersonic flows, both the *iSol* model and the Zweifel correlations do not provide the same optimal solidity value minimizing the overall loss that has been computed using CFD simulations. This is due to the inherent limitations of both models, which account for the passage loss only and rely on the incompressible flow assumption. For the *Aachen* blade, the transonic and supersonic cases also exhibit a higher value of the optimal solidity obtained by minimizing only the passage losses. In this blade, passage losses are affected by the presence of a reflected shock on the rear side of the suction side, which largely influences the value of the optimal solidity.

Figures 12a and 13a show the trends of $C_{pb}t/s$ as a function of the axial solidity obtained from the CFD simulations for all the cases listed in Table 2, and for the *iMM-Kis3* and the *Aachen* blades, respectively. Figures 12b–d and 13b–d, instead, show the trends of θ/s, $(\delta^* + t)^2/s^2$, and θ^*/s as a function of the axial solidity for the *iMM-Kis3* and the *Aachen* blades, respectively. The trends of the mixing losses observed in Figures 7 and 8 are aligned with those of the three boundary layer parameters. No correlation is instead observed with the trends of the base pressure coefficient. It can then be argued that mixing losses are mainly a function of the state of the boundary layer at the trailing edge, which, in turn, is affected by the fluid molecular complexity and the thermodynamic state. Among the four parameters, the momentum and kinetic energy thickness trends exhibit a strong correlation with those observed for both the mixing and the overall loss: for both parameters, the

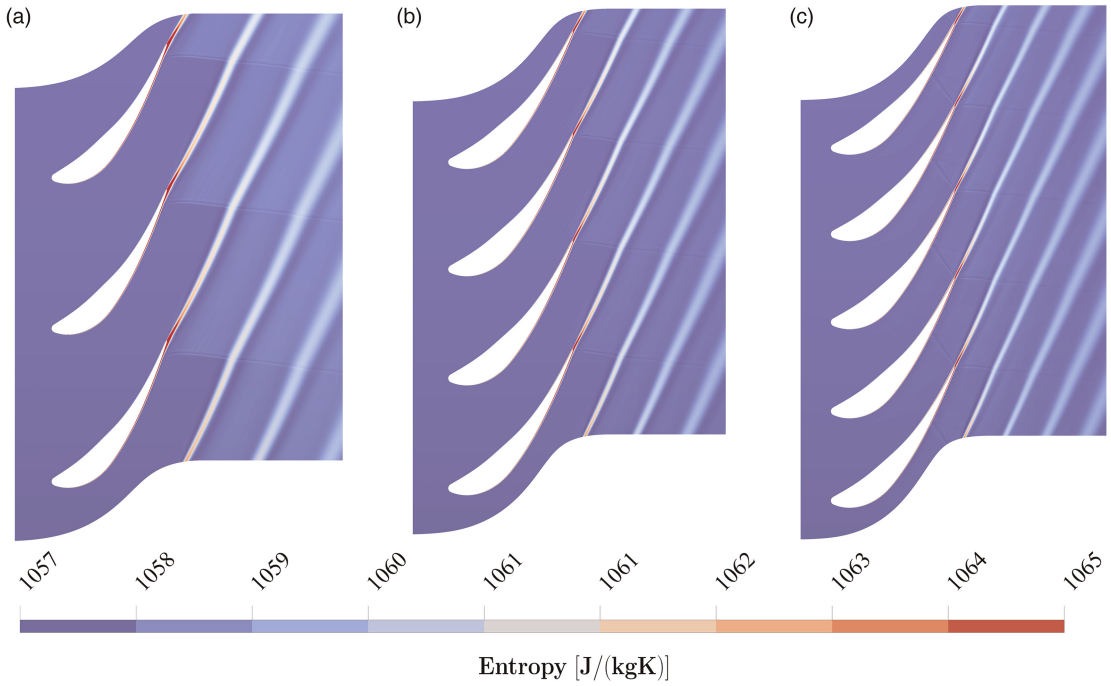

Figure 9. Entropy field in the proximity of the blade trailing edge for the case iMM, $\beta_{ts} = 1.7$. (a) $\sigma_x \simeq 0.65$, (b) $\sigma_x \simeq 1.05$, (c) $\sigma_x \simeq 1.4$.

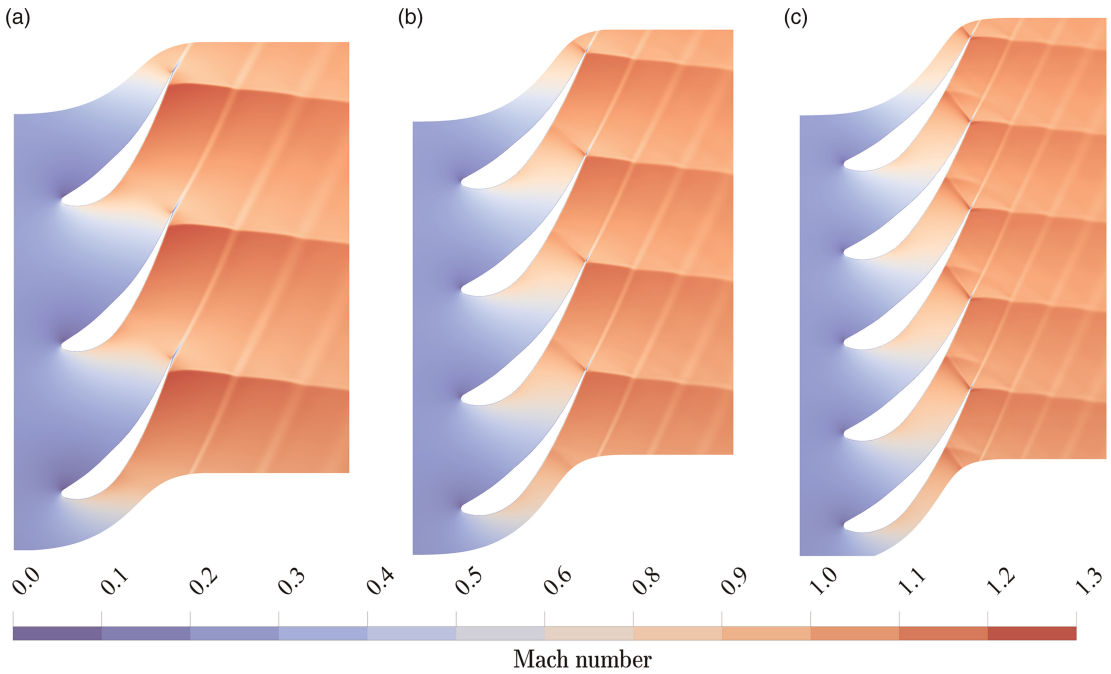

Figure 10. Mach number field in the proximity of the blade trailing edge for the case iMM, $\beta_{ts} = 1.7$. (a) $\sigma_x \simeq 0.65$, (b) $\sigma_x \simeq 1.05$, (c) $\sigma_x \simeq 1.4$.

minimum of the curves shifts towards larger solidity values at higher cascade Mach numbers, and the corresponding σ_x values are in line with the $\sigma_{x,\mathrm{opt}}$ ones obtained from the CFD results (Figures 7 and 8). Moreover, similarly to what has been observed for the loss breakdown, the fluid molecular complexity and the thermodynamic state move the minimum of both θ/t and θ^*/t towards larger σ_x values in the transonic and supersonic regimes. Regarding the displacement thickness, the subsonic and transonic cases follow the same trend as that of the overall loss and those of the other boundary layer integral quantities; conversely, the supersonic cases exhibit a

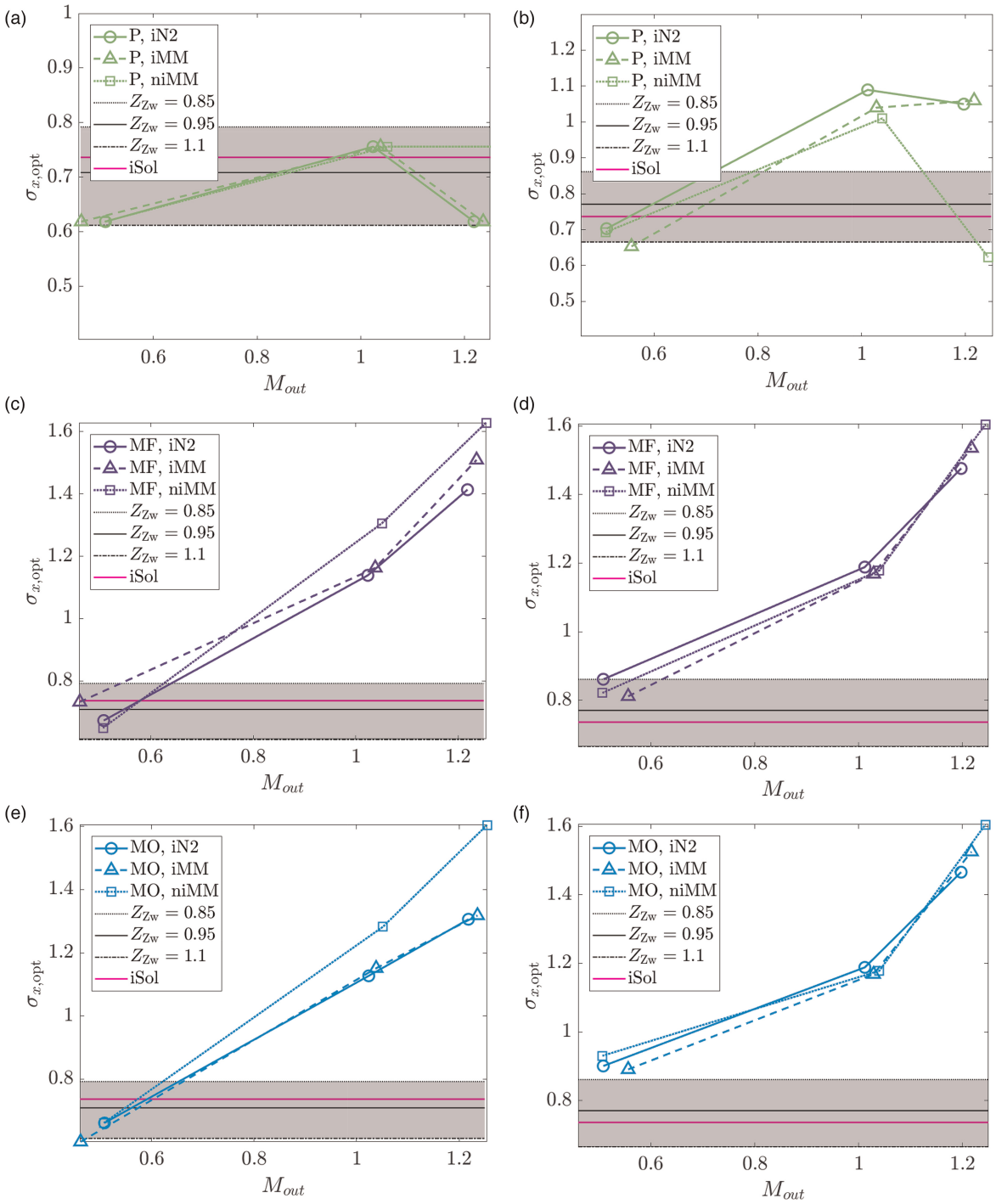

Figure 11. Optimal solidity vs outlet Mach number for (a–e) the *iMM-Kis3* and (b–f) the Aachen blades. The values predicted by the reduced-order model (ROM) and the Zweifel correlation for three different values of the Z_{ZW} are also displayed. The region of validity of the Zweifel correlation for $Z_{ZW} = 0.8 - 1.1$ is also highlighted in blue. $\sigma_{x,opt}$ values have been estimated considering (a) and (b) passage losses, (c) and (d) overall mass flow averaged losses and (e) and (f) overall mixed-out averaged losses. (a) *iMM-Kis3* (b) Aachen (c) *iMM-Kis3* (d) Aachen (e) *iMM-Kis3* (f) Aachen.

minimum at $c_{ax}/s \sim 0.8$ for the *iMM-Kis3* blade, while no minimum is observed in the *Aachen* blade case. However, the contribution of the displacement thickness is smaller in magnitude compared to that of the momentum and kinetic energy thickness.

Figure 14a shows the contour plot of the computed optimal solidity values as a function of the flow angles calculated with the *iSol* model. These variations of optimal solidity are compared with those computed with the Zweifel correlation using two different values of the Zweifel coefficient (Figure 14b and c). It can be observed that the optimal σ_x trends are very similar, regardless of the model with which they are computed. At fixed α_1

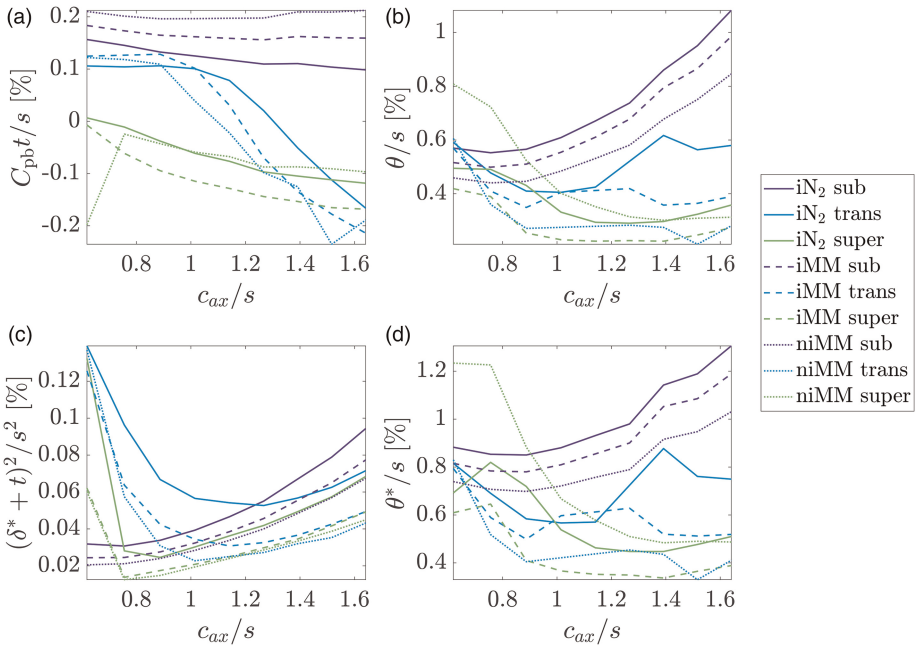

Figure 12. Normalized trends of (a) base pressure coefficient, (b) momentum thickness, (c) displacement thickness, and (d) kinetic energy thickness in the proximity of the trailing edge vs axial solidity for the *iMM-Kis3* blade. The boundary layer integral parameters are estimated by summing the contributions of both the pressure and the suction side.

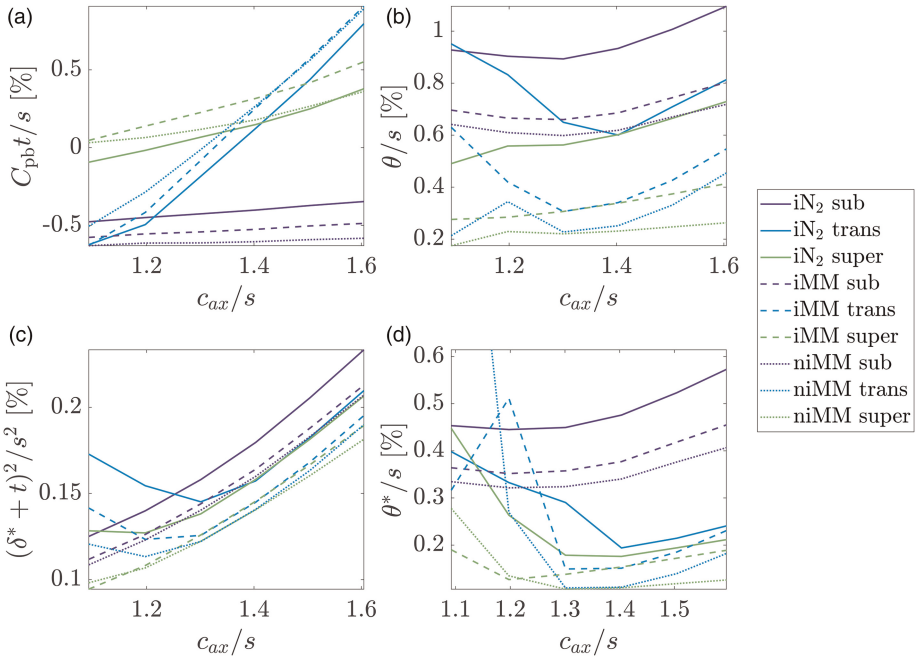

Figure 13. Normalized trends of (a) base pressure coefficient, (b) momentum thickness, (c) displacement thickness, and (d) kinetic energy thickness in the proximity of the trailing edge vs axial solidity for the Aachen blade. The boundary layer integral parameters are estimated by summing the contributions of both the pressure and the suction side.

and α_2, the optimal solidity value obtained with *iSol* is within the bounds defined by the values obtained with the Zweifel correlation for $Z_{Zw} = 0.8$ and $Z_{Zw} = 1.1$.

Figure 15 shows the results obtained with the *cSol* model for both the *iMM-Kis3* and the *Aachen* blades for the test cases listed in Table 2. The optimal solidity values obtained with the model are compared against those

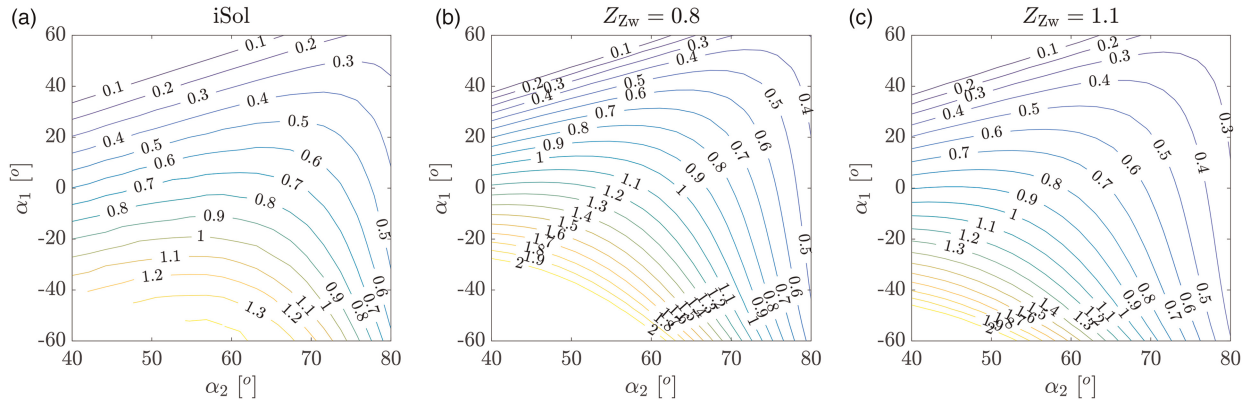

Figure 14. Optimal solidity σ_x vs flow angles resulting from (a) the *iSol* model, and the Zweifel correlation assuming (b) $Z_{Zw} = 0.8$ and (c) $Z_{Zw} = 1.1$.

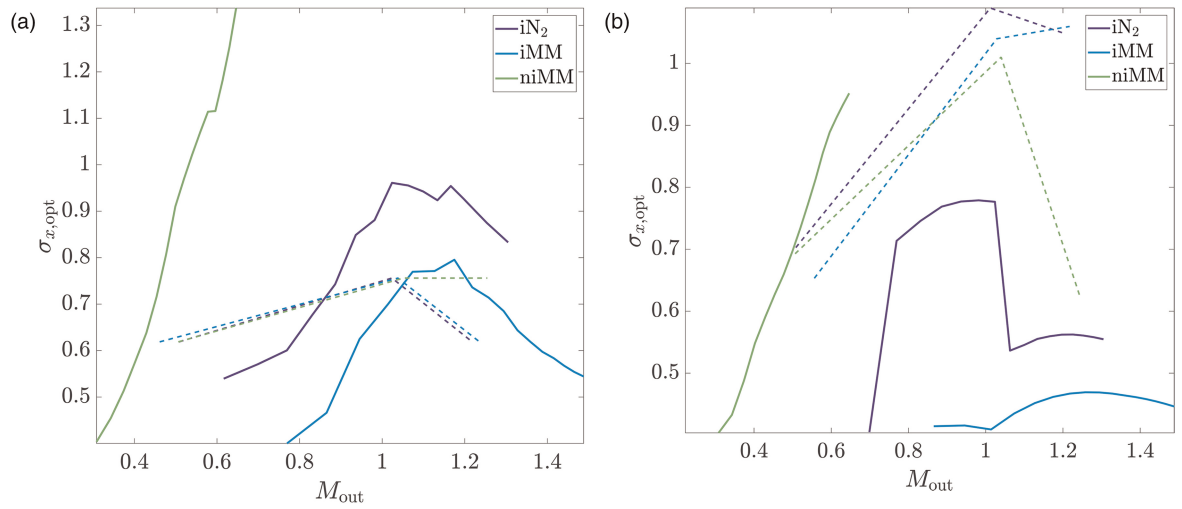

Figure 15. Optimal solidity value estimations vs outlet Mach number for (a) the *iMM-Kis3* and (b) the Aachen blades, respectively. Results obtained with the compressible reduced-order model and the numerical simulations are depicted in solid and dashed lines, respectively.

obtained from CFD considering only the passage loss calculated up to the trailing edge. For the iN_2 case and the *iMM* one (*iMM-Kis3* blade only), the trend with the Mach number is somewhat in agreement with that obtained with the CFD: both curves exhibit a maximum at transonic conditions, i.e., $M_{\mathrm{out}} \sim 1$. However, the absolute values are incorrectly estimated. Predictions and values are instead inaccurate for all the remaining cases: the model fails to match the trends obtained from CFD. In particular, for both the investigated blades, the model does not provide reliable results for the *niMM* case beyond $M_{\mathrm{out}} > 0.6$, and, for the *Aachen* blade, iN_2 and *iMM* cases, the model fails if $M_{\mathrm{out}} > 1$. The outcome of this analysis points out that the physics of the problem is not correctly modelled: the possible causes of error can be attributed to (i) excessively simplified blade loading distribution; (ii) inaccurate C_d value, especially in the presence of strong stream-wise pressure gradients; (iii) inability to capture the effect of boundary layer-shock interaction in the compressible flow regime, which results in additional passage loss.

Finally, Figure 16a–c shows the mixing loss as a function of the solidity for the iN_2, *iMM*, and *niMM* cases, respectively. Calculations have been performed for the *iMM-Kis3* blade only. The mixing loss has been estimated using the control volume-based approach described in Section 2 using as input the base pressure coefficient and the boundary layer integral parameters obtained from CFD and shown in Figure 12. For all three cases, the control volume-based model provides a trend of mixing losses with the solidity which is aligned with that obtained from the RANS calculations up to the transonic regime: the minimum of the mixing losses shifts towards higher σ_x as the outlet Mach number increases. This further corroborates the finding that the mixing losses, and, thus, the optimal solidity value, are strongly affected by the state of the boundary layer at the trailing

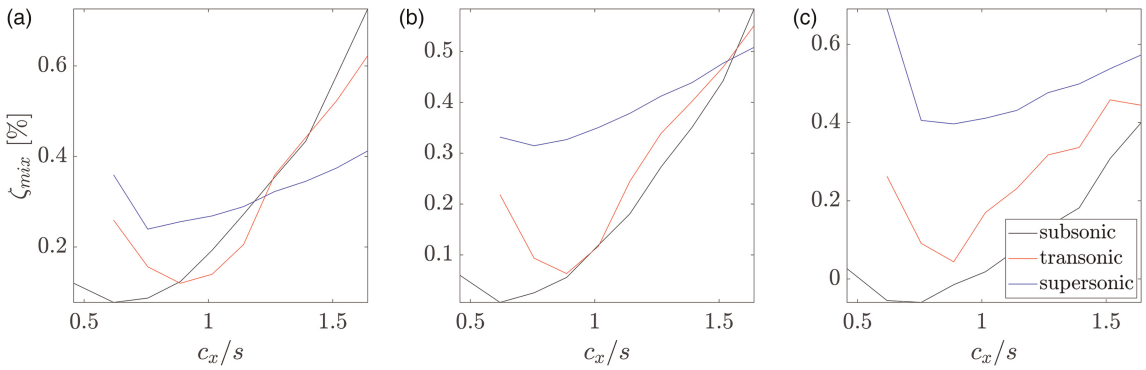

Figure 16. Mixing losses computed using the control volume-based model described in Section 2 vs axial solidity for the *iMM-Kis3* blade. Each graph refers to the (a) air, (b) iMM, and (c) niMM cases, respectively.

edge. However, the results for the supersonic regime are not consistent with those obtained from CFD simulations: in particular, the minimum of the mixing losses is located at lower solidity values than those obtained for the transonic case. The model does not account for the loss induced by the fish-tail shock waves forming downstream of the blade trailing edge. In conclusion, the proposed control volume approach for the prediction of the optimal solidity value is incapable of modelling physical phenomena with a sufficient degree of detail, and the optimal solidity value can only be predicted by numerical simulations or experiments.

Conclusions and Outlook

The optimal solidity value is used to determine the number of blades of an axial turbine stage. The work here presented aimed at investigating the influence of the molecular complexity of the working fluid, its thermodynamic state, and flow compressibility on the optimal solidity, as well as developing reduced-order models which can be used to estimate its value during the preliminary design. The optimal solidity values provided by the Zweifel criterion have been compared against those obtained with two-dimensional CFD simulations of the flow around two representative turbine stator blade geometries. A loss breakdown analysis based on data obtained from the CFD simulations has also been carried out. Reduced-order models for the estimation of the optimal solidity value based on the minimization of the passage losses in the incompressible (**iSol**) and compressible (**cSol**) regimes have been developed and applied to selected test cases.

Based on the results of the study, the following conclusions can be summarized.

- Both the Zweifel correlation and the reduced-order incompressible flow model (**iSol**) predict inaccurate values of the optimal solidity because they do not account for the mixing loss, which is the primary loss if the flow is transonic or supersonic.
- The higher the cascade outlet Mach number, the higher the optimal solidity value, regardless of the working fluid.
- In the case of transonic and supersonic cascades, the optimal solidity value increases with the molecular complexity of the working fluid. However, this effect is negligible compared to that of the flow compressibility.
- If the working fluid is in a dense vapor state (with a non-negligible departure from ideal gas states), the mixing loss largely prevails over the passage loss, and the optimal solidity value further increases compared to that estimated under the assumption of a dilute gas.
- The compressible flow model (**cSol**), which has been developed for the compressible turbine flow case and is based on the minimization of the passage losses, fails to predict the correct trends and accurate values of optimal solidity.
- The accurate estimation of optimal solidity values requires the development of models and correlations for the estimation of the integral parameters of the boundary layer at the blade trailing edge and the accounting of the mixing losses in the wake region.
- For a turbine stage operating in the transonic regime $M_{\text{out}} \sim 1$, the results of the numerical investigation show that the minimum of the overall loss is found for $1 < \sigma_{x,\text{opt}} < 1.2$. If the Zweifel correlation is used in the preliminary design, values of the Z_{Zw} coefficient lower than those conventionally recommended in literature have to be employed ($Z_{Zw} < 0.7$). This would result in turbine stages with a larger number of blades, entailing an increase in efficiency at the expense of a larger amount of needed material to manufacture the stage.

The research documented in this paper is the first step toward the development of novel design guidelines for the selection of the optimal solidity of axial and radial Organic Rankine Cycle (ORC) turbines. Future efforts will involve the development of a model for the estimation of the integral parameters of the boundary layer at the blade trailing edge and the implementation of the model described in Pini and De Servi (2020) for the calculation of the dissipation coefficient C_d.

Nomenclature

Symbols

b Blade camber
c Blade chord/1st scaling parameter for pressure distribution
C_{pb} Base pressure coefficient
C_d Dissipation coefficient
$\mathrm{d}V$ 2nd scaling parameter for velocity distribution
$\mathrm{d}p$ 2nd scaling parameter for pressure distribution
h Specific enthalpy
k 1st scaling parameter for velocity distribution
M Mach number
$\dot{m}$ Mass flow rate
o Throat length
p Pressure
Re Reynolds number
s Specific entropy/Blade pitch
T Temperature
t Trailing edge thickness
V Absolute velocity
v Specific volume
Z Compressibility factor
Z_{Zw} Zweifel coefficient
α Absolute flow angle
α_m Blade metal angle at trailing edge
β_{ts} Total-to-static expansion ratio
γ Ratio of specific heats
γ_{pv} Generalized isentropic pressure-volume exponent
δ^* Displacement thickness
ζ Loss coefficient
θ Momentum thickness
θ^* Kinetic energy thickness
ρ Density
σ_x Blade axial solidity
χ Gauge angle

Subscripts

e Mixed-out state
out Outlet (CFD)
opt Optimal
P Passage
ps Pressure side
s Entropy-related
ss Suction side
t Stagnation quantity
te Trailing edge
ts Total-to-static

x Axial component
y Tangential component
∞ Dilute gas state ($v \to \infty$)
1 Inlet
2 Outlet

Abbreviations

CFD Computational fluid dynamics
CO^2 Carbon dioxide
MF Mass-flow average
MIX Mixing
MM Hexamethyldisiloxane
MO Mixed-out averaged
P Passage
RANS Reynolds averaged Navier-Stokes
ROM Reduced-order model

Funding sources

This research has been supported by the Applied and Engineering Sciences Domain (TTW) of the Dutch Organization for Scientific Research (NWO), Technology Program of the Ministry of Economic Affairs, grant # 15837.

Competing interests

Francesco Tosto declares that he has no conflict of interest. Piero Colonna declares that he has no conflict of interest. Matteo Pini declares that he has no conflict of interest.

References

ANSYS. (2019). Ansys workbench, release 19.3, ANSYS, canonsburg, pa.

Baumgärtner D., Otter J. J., and Wheeler A. P. S. (2020). The effect of isentropic exponent on transonic turbine performance. *Journal of Turbomachinery*. 142 (8): 081007. https://doi.org/10.1115/1.4046528.

Colonna P., Casati E., Trapp C., Mathijssen T., Larjola J., et al. (2015). Organic rankine cycle power systems: from the concept to current technology, applications, and an outlook to the future. *Journal of Engineering for Gas Turbines and Power*. 137 (10): 100801. https://doi.org/10.1115/1.4029884.

Coull J. D. and Hodson H. P. (2013). Blade loading and its application in the mean-line design of low pressure turbines. *Journal of Turbomachinery*. 135 (2): 021032. https://doi.org/10.1115/1.4006588.

Denton J. D. (1993). The 1993 IGTI scholar lecture: loss mechanisms in turbomachines. *Journal of Turbomachinery*. 115 (4): 621–656. https://doi.org/10.1115/1.2929299.

Doughty R., Moses H., and Gregory B. (1992). The effect of blade solidity on the aerodynamic loss of a transonic turbine cascade. In 30th Aerospace Sciences Meeting and Exhibit, American Institute of Aeronautics and Astronautics, Reno, NV, USA.

Giuffré A. and Pini M. (2021). Design guidelines for axial turbines operating with non-ideal compressible flows. *Journal of Engineering for Gas Turbines and Power*. 143 (1): 011004. https://doi.org/10.1115/1.4049137.

Knowledge Center on Organic Rankine Cycle (KCORC). (2022). Thermal Energy Harvesting - the Path to Tapping into a Large CO_2-free European Power Source, Thermal Energy Harvesting Advocacy Group White Paper.

Kouremenos D. A. and Antonopoulos K. A. (1987). Isentropic exponents of real gases and application for the air at temperatures from 150 K to 450 K, Acta Mech. 65(1–4), 81–99. https://doi.org/10.1007/BF01176874.

Lemmon E. W., Bell I. H., Huber M. L., and McLinden M. O. (2018). NIST standard reference database 23: Reference fluid thermodynamic and transport properties-REFPROP, version 10.0, National Institute of Standards and Technology.

Menter F. R. (1994). Two-equation eddy-viscosity turbulence models for engineering applications. *AIAA Journal*. 32 (8): 1598–1605. https://doi.org/10.2514/3.12149.

Otero R. G. J., Patel A., Diez S. R., and Pecnik R. (2018). Turbulence modelling for flows with strong variations in thermo-physical properties. *International Journal of Heat and Fluid Flow*. 73: 114–123. https://doi.org/10.1016/j.ijheatfluidflow.2018.07.005.

Pini M. and De Servi C. (2020). Entropy generation in laminar boundary layers of non-ideal fluid flows. In Non-Ideal Compressible Fluid Dynamics for Propulsion and Power: Lecture Notes in Mechanical Engineering, pp. 104–117.

Romei A., Vimercati D., Persico G., and Guardone A. (2020). Non-ideal compressible flows in supersonic turbine cascades. Journal of Fluid Mechanics. 882: A12. https://doi.org/10.1017/jfm.2019.796

Stephan B., Gallus H. E. and Niehuis R. (2000). Experimental investigations of tip clearance flow and its influence on secondary flows in a 1-1/2 stage axial turbine. In: Aircraft Engine, Marine, Turbomachinery, Microturbines and Small Turbomachinery, Vol. 1. Munich, Germany: American Society of Mechanical Engineers.

Tosto F., Giuffré A., Colonna P. and Pini M. (2021). Non-ideal effects in compressible swirling flows, In Proceedings of the 3rd International Seminar on Non-Ideal Compressible Fluid Dynamics for Propulsion and Power, edited by Pini M., De Servi C., Spinelli A., di Mare F., and Guardone A. Cham: Springer International Publishing. Vol. 28, pp. 36–43. Series Title: ERCOFTAC Series.

Traupel W. (1966). Thermische Turbomaschinen. Berlin Heidelberg: Springer.

Wilson D. G. (1987). New guidelines for the preliminary design and performance prediction of axial-flow turbines. Proceedings of the Institution of Mechanical Engineers, Part A: Power and Process Engineering. 201 (4): 279–290. https://doi.org/10.1243/PIME_PROC_1987_201_035_02.

Zweifel O. (1945). The spacing of turbo-machine blading especially with large angular deflection. Brown Boveri Review. 32 (12), 436–444.